

## Influence of MgO nanoparticles on the physiochemical, transport, and antimicrobial properties of polyethersulfone membranes

Paulina Sienkiewicz\*, Dominika Darowna, Manu Jose, Michał Zgrzebnicki, Agata Markowska-Szczupak, Sylwia Mozia

Faculty of Chemical Technology and Engineering, Institute of Inorganic Chemical Technology and Environment Engineering, West Pomeranian University of Technology, Pułaskiego 10, 70-322 Szczecin, Poland, Tel. +48 91 449 47 30; email: paulina.sienkiewicz@zut.edu.pl

Received 18 April 2018; Accepted 18 June 2018

### ABSTRACT

In this study the influence of the addition of MgO nanoparticles (NPs) on physiochemical, transport, separation, and antimicrobial properties of polyethersulfone (PES) membranes was investigated. The MgO NPs with the agglomerate size of ca. 139 nm and the isoelectric point of 12.4 were obtained by the sol-gel technique. The unmodified membrane (A1, 15 wt.% PES) and membranes modified with different concentrations of MgO NPs (0.1–5 wt.% in relation to PES) were obtained by the wet phase inversion method using water as a nonsolvent and *N,N*-dimethylformamide as a solvent. The highest permeability values (209 dm<sup>3</sup>/m<sup>2</sup>h bar) were noted for a membrane containing 5 wt.% of MgO NPs (A6). A decrease of porosity from 75% (A1) to 70% (A6) and contact angle values from 59.2° (A1) to 46.6° (A6) with the increasing concentration of MgO NPs was observed. The isoelectric point was higher for the modified membranes (pH(I) = 3.4–3.6) compared with the unmodified one (2.8). Atomic force microscopy analysis revealed a significant difference between the surface roughness of the unmodified (1.75 nm) and modified membranes (2.84–2.60 nm). The highest inhibition of *Escherichia coli* growth was observed for the membrane modified with 5 wt.% MgO NPs, in case of which the bacterial cell viability was reduced by ca. 50%.

*Keywords:* Biofouling; Polyethersulfone membrane; Magnesium oxide nanoparticles; *Escherichia coli*; Antimicrobial activity

### 1. Introduction

A rapid development of membrane technologies during last decades has resulted in their wide application in many fields, including water and wastewater treatment, biotechnology, food processing, life science, and energy conversion [1–4]. Despite a great progress in the development of membrane processes, to this day the phenomenon of fouling is still one of the main drawbacks of these techniques. Fouling is responsible for a decrease of permeate flux and a shortening of a lifespan of membranes. Depending on the type of a foulant, various types of fouling can be distinguished: scaling caused by inorganic species, organic fouling, colloidal fouling,

and biofouling. Biofouling results of the deposition and the growth of microorganisms on the surface of a membrane. It is one of the most troublesome phenomenon occurring during membrane processes, because it is associated with microorganisms, which divide and grow at a very fast rate.

Over the years, numerous methods have been proposed to limit the development of biofilms. One of the most commonly used is based on the application of biocides into the feed water. However, some biocides, such as ozone or chlorine, can act adversely on polymeric membranes by damaging their structure. Moreover, under the action of the oxidizing agents, various harmful intermediate products such as trihalomethanes, haloacetic acids, and bromates can be formed [5,6]. Furthermore, the application of biocides does

\* Corresponding author.

not allow to completely eliminate biofouling phenomenon. Other attempts aimed at biofouling reduction are based on mechanical removal of the resulting biofilm, using, for example, an automatic scrubber or high-pressure cleaning [7]. Nevertheless, these methods are complicated, require a lot of work effort and generate high costs, all making the process unattractive.

Due to these limitations, the researchers focus on the development of novel solutions of reduction of membrane fouling. One of the most common attempts is modification of a membrane surface or a membrane structure. In the former case, the applied techniques include [8,9]: grafting methods (photo-initiated grafting, redox-initiated grafting, enzymatic grafting, initiated chemical vapor deposition), plasma treatment methods (modification in plasma of nonpolymerizable gases, modification in plasma of polymerizable molecules, plasma-induced grafting), physical coating/adsorption of a thin layer of water-soluble polymers or surfactants on a membrane surface (coating via casting, adsorption, or filtration), and methods based on chemical reactions on a membrane surface. These methods are rather complex and usually the effect is still too poor to ensure a satisfactory reduction of membrane fouling [10]. Therefore, another attempt based on the additive blending methods seems to be more attractive. In these methods the selected modifiers are introduced directly into the casting solution, without the need of multistage procedures involvement during the preparation of membrane. Recently, the expanding growth of nanotechnology has created a new opportunity to prepare mixed matrix membranes with unique properties. Nanoparticles (NPs), such as  $\text{TiO}_2$ ,  $\text{SiO}_2$ ,  $\text{Al}_2\text{O}_3$ , halloysite nanotubes, carbon nanomaterials including single- and multiwalled nanotubes, graphene, and fullerenes have been proposed as modifiers [11,12]. In general, the modified membranes exhibit improved permeability and higher fouling resistance than the unmodified ones [12].

Another group of nanomodifiers consists of metallic NPs, such as Ag, Cu, Au, and Pd [13–15]. It was reported that these NPs significantly improved the biocidal properties of polymeric membranes [16]. However, the production of metallic NPs is usually complicated, which makes them a rather expensive additive. Moreover, the main problem associated with the modification of membranes with NPs is their stability. Metallic NPs are usually easily released from the membrane, which does not only lead to a loss of membrane properties, but it may also create a danger of a recontamination of water and the environment [17].

Recently, magnesium oxide nanoparticles (MgO NPs) have gained significant attention of researchers. Nanosized MgO is relatively cheap, environment and human-friendly. Furthermore, it has been reported that MgO NPs are characterized by a similar level of antimicrobial activity against Gram-negative and Gram-positive bacteria as the most commonly discussed Ag and Cu NPs [18]. The production of nanosized magnesium oxide particles is simple, due to the availability of natural materials, which makes this type of the modifying agent especially attractive [19]. Among the three main methods of synthesis of MgO NPs: sol-gel, hydrothermal, and micro-emulsion, the former two methods are the most often used by scientists [20].

Despite numerous advantages of MgO NPs, there are only a few works on their use for the production of

polymeric membranes for water/wastewater treatment. Arumugham et al. [21] reported that addition of MgO NPs into the sulfonated polyphenyl sulfone/polyphenyl sulfone (MgO/SPPSU/PPSU) led to an improvement of rejection, permeability, and hydrophilicity of membranes as well as their oleophobicity against oil/water emulsion. Hosseini et al. [22] reported dependence between different concentrations of MgO NPs and enhancement of the permeability and antifouling properties of polyethersulfone (PES) nanofiltration membranes.

In spite of the widely described antimicrobial properties of MgO NPs, however, there is lack of information in the literature related to the effect of the addition of these NPs on the antimicrobial properties of polymeric membranes used in micro- and ultrafiltration. Therefore, the objective of the present research was to evaluate the influence of MgO NPs on the antimicrobial performance of PES membranes obtained by the wet phase inversion method. *Escherichia coli* was selected as a model microorganism. The influence of the addition of nanosized MgO on the permeate flux, hydrophilicity, porosity, and membrane morphology was also investigated.

## 2. Experimental

### 2.1. Materials

Polyethersulfone (VERADEL PESU, Solvay, Belgium) was provided by Solvay Polska Sp. z o.o. *N,N*-Dimethylformamide (DMF, puriss p.a.),  $\text{MgCl}_2 \times 6\text{H}_2\text{O}$  (puriss p.a.) and NaOH (puriss p.a.) were purchased from Avantor Performance Materials Poland S.A. Polyethylene glycol (PEG, molecular weight 8 kDa) was purchased from Merck, Germany.

During microbial tests, NaCl supplied by Chempur (Poland) and plate count agar (PCA) purchased from BIOCORP (Poland) were used. The Gram-negative *E. coli* (bacteria strain K12, ATCC 29425, USA) were selected as model microorganisms. The initial concentration of a bacteria suspension was set at a turbidity of 0.5 according to McFarland scale (McFarland standards, bioMérieux, France).

In all experiments pure (deionized) water (type 2, 0.066  $\mu\text{S}/\text{cm}$ ) (Elix 3, Millipore) was applied.

### 2.2. Preparation of MgO NPs

MgO NPs were prepared by the sol-gel technique described by Moussavi et al. [19] with some modifications. First, 100 g of  $\text{MgCl}_2 \times 6\text{H}_2\text{O}$  was dissolved in 1  $\text{dm}^3$  of distilled water, and then 50  $\text{cm}^3$  of 1 M NaOH solution was added dropwise. The obtained solution was stirred at 250 rpm for 4 h to produce magnesium hydroxide sediment. After that, the suspension was separated by Universal 320R separator (Hettich, Germany) at 3,000 rpm for 5 min, washed three times with water and finally dried at 60°C for 24 h. The dry powder was calcined in a muffle furnace (Nabertherm GmbH, Germany) in air at 450°C for 2 h to prepare MgO NPs.

### 2.3. Preparation of membranes

Membranes were prepared via the wet phase inversion method using PES as a polymer, DMF as the polymer solvent, and water as the nonsolvent. The composition of

Table 1  
Composition of casting solutions

Sample code	PES:DMF	MgO NPs (wt.% in relation to PES)
A1	15:85	0
A2	15:85	0.1
A3	15:85	1
A4	15:85	2
A5	15:85	3
A6	15:85	5

casting solutions is summarized in Table 1. In case of the unmodified PES membrane (A1), the casting dope was obtained by the dissolution of 8.38 g PES in 50 cm<sup>3</sup> of DMF. After degassing, the casting solution was casted on a glass plate using an automatic film applicator (Elcometer 4340, Elcometer Ltd., UK). The knife gap was set at 0.1 mm. The casted film was immersed in the water coagulation bath at 20°C for 24 h.

The membranes modified with MgO NPs were prepared from casting dopes containing 0.1, 1, 2, 3, or 5 wt.% of the nanomaterial in relation to PES (Table 1). The membranes were denoted later as A2–A6, respectively. The procedure of preparation of casting dope was as follows. A suspension of a defined amount of MgO NPs in DMF (10 cm<sup>3</sup>) obtained using ultrasonic liquid processor (Vibra-cell VCX-130, Sonics, USA; output power 130 W, frequency 20 kHz, amplitude 80%, time of sonication 30 min) equipped with a 6 mm ultrasonic probe, was added to the solution of PES (8.38 g) in DMF (40 cm<sup>3</sup>). Such obtained casting solution was stirred (200 rpm) at a temperature of 55°C–60°C for 15 min and subsequently sonicated in ultrasonic bath at a temperature of 20°C–25°C for 15 min. Both steps, that is, stirring and sonication were repeated in turns for 2 h. Membranes were casted on a glass plate according to the procedure described earlier.

#### 2.4. Characterization of MgO NPs and membranes

The phase composition of the MgO NPs was determined based on X-ray diffraction (XRD) analysis (PANalytical Empyrean X-ray diffractometer) using CuK $\alpha$  radiation ( $\lambda = 1.54056 \text{ \AA}$ ). The size and the zeta potential of MgO NPs were measured using Zetasizer Nano ZS (Malvern, UK).

The porosity of membranes was evaluated using gravimetric method and calculated according to Eq. (1) as follows:

$$P = \frac{(m_{\text{wet}} - m_{\text{dry}}) / \rho_w}{(m_{\text{wet}} - m_{\text{dry}}) / \rho_w + m_{\text{dry}} / \rho_p} \times 100\% \quad (1)$$

where  $m_{\text{dry}}$  and  $m_{\text{wet}}$  are weights (g) of dry and wet membrane samples, respectively;  $\rho_w$  is water density at 20°C ( $\rho_w = 0.9982 \text{ g/cm}^3$ ); and  $\rho_p$  is PES density ( $1.37 \text{ g/cm}^3$ ).

The contact angle of PES membranes was measured by depositing a water drop (10  $\mu\text{L}$ ) on the surface of the sample. The goniometer model 260 (ramé-hart instruments co., USA) was used to record the results. The received contact angle values were calculated as an average of at least 10 measurements made for 3 different membrane pieces.

The isoelectric point of obtained membranes was determined using SurPASS 3 analyzer (Anton Paar, Austria). 0.001 M KCl solution in ultrapure water (Simplicity<sup>®</sup>, Millipore) was used as an electrolyte. The pH was controlled using HCl and KOH solutions.

Atomic force microscopy (AFM) was applied during investigations of the topography of the membranes surface. NanoScope V Multimode 8 scanning probe microscope (Bruker Corp., Germany) was used for the AFM analysis. Measurements were made with the silicon nitride ScanAsyst – Air probe in the ScanAsyst mode, which used the so-called Peak Force Tapping Mechanism. The scanned area was  $10 \mu\text{m} \times 10 \mu\text{m}$ .

Cross-sections and surfaces of membrane samples were examined using Hitachi SU8020 ultra-high resolution field emission scanning electron microscope (SEM). Before analysis, membranes were dehydrated in a number of soaking solutions consisting of ultrapure water and ethanol (concentrations of ethanol: 0, 20, 40, 60, 80, and 96 vol.%). For the cross-sectional examination, membranes were crushed in liquid nitrogen. Before measurements, membranes' samples were attached on a table using a carbon tape and they were coated with a 5 nm thick chromium layer (Q150T ES coater, Quorum Technologies Ltd., UK). Two types of analysis modes were used: utilizing secondary electrons (SEs) and back scattered electrons (BSEs). Accelerating voltage for SE mode was 5 kV and for BSE mode 15 kV.

Water transport properties of developed membranes were determined using a laboratory-scale ultrafiltration installation. The installation was equipped with a needle valve with manometer, stainless steel membrane module (with a 1.194 mm feed spacer), and a plunger pump with a pressure dampener. The membrane effective area was 0.0025 m<sup>2</sup>. The pure water flux was measured at the transmembrane pressure of 1, 2, or 3 bar and at the feed cross-flow velocity ( $v$ ) of 0.5 m/s. The temperature was maintained at  $20^\circ\text{C} \pm 1^\circ\text{C}$ . The value of the permeate flux was evaluated based on the volume of liquid permeating through the membrane during a defined period of time. Each experiment was repeated at least two times.

#### 2.5. Microbiological study

##### 2.5.1. Preparation of culture media

PCA solution prepared according to procedures given by the manufacturer was poured into sterile plastic Petri dishes and left to solidify. After that, plates were sterilized under UVC light for 20 min and dried in the incubator at a temperature of 30°C. A saline solution was prepared by the dissolution of 8.5 g of NaCl in 1 dm<sup>3</sup> of water and the sterilization in an autoclave.

##### 2.5.2. Bacteria counting

For counting of bacteria, a series of decimal dilutions in the saline solution were prepared. 0.3 cm<sup>3</sup> of an appropriate diluted solution was evenly spread around the plate containing PCA using a sterile spreader. Three replications for each dilution were made. Plates were incubated at 37°C for 24 h. After the incubation, visible colonies of bacteria on agar plates were counted using the counter (LKB 2002,

POL-EKO, Poland). The average colony forming unit (CFU) per  $\text{cm}^3$  values were calculated as follows:

$$\text{CFU} / \text{cm}^3 = \frac{X \times Y}{Z} \quad (2)$$

where  $X$  – number of colonies visible on the Petri dish,  $Y$  – total dilution factor, and  $Z$  – volume of bacteria suspension placed on the agar ( $0.3 \text{ cm}^3$ ).

### 2.5.3. Study of antibacterial properties of polymeric membranes

A dry piece of a membrane ( $12.5 \text{ cm} \times 4.5 \text{ cm}$ ), previously dehydrated in ethanol, was sterilized in an autoclave. After that, it was put into a Duran glass bottle containing  $100 \text{ cm}^3$  of bacteria suspension (turbidity of 0.5 according to the McFarland scale). Then, an ellipsoidal stirrer (diameter 12 mm, length 25 mm) was added. Bottles with bacteria and the membrane were placed on a magnetic stirrer at  $37^\circ\text{C}$  for 24 h. The mixing speed was set at 250 rpm. After the incubation, three samples were taken from each bottle and the degree of bacteria degradation was determined using the dilution method described earlier. Blank test was carried out under the same conditions, although without a membrane inside the bottle. The degradation values presented in the discussion were evaluated with reference to the blank sample.

## 3. Result and discussion

### 3.1. Characteristics of MgO NPs

Fig. 1 shows the XRD diffractogram of MgO NPs. Peaks at  $2\theta$  angle corresponding to reflection planes (111), (200), (220), (311), and (222) could be observed. The noted reflections were characteristic for the cubic structure of MgO and could be assigned for pure MgO phase (ICDD 04-002-2876). The average size of crystallites ( $D$ ) was calculated using the Scherrer equation (3) as follows:

$$D = \frac{K\lambda}{\beta \cos\theta} \quad (3)$$

where  $K$  is the shape factor ( $K = 0.9$ ),  $\lambda$  is the wavelength of  $\text{CuK}\alpha$  radiation ( $\lambda = 1.54056 \text{ \AA}$ ), and  $\beta$  is the mean full width at the half maximum height of the diffraction peak.

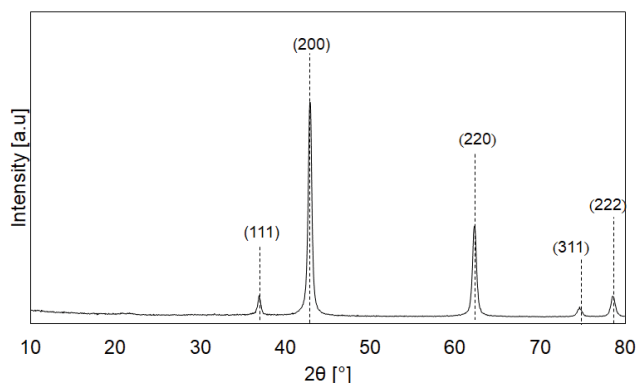


Fig. 1. XRD pattern of prepared MgO NPs.

The XDR analysis revealed that the crystallite size of MgO NPs was 21.5 nm.

MgO NPs exhibited elliptical or oval shapes with dimensions in the range of 62.5–112.5 nm, as it was found based on SEM analysis (Fig. 2). The average size of MgO NPs agglomerates measured using Zetasizer Nano ZS was  $139 \pm 19 \text{ nm}$  and the isoelectric point (pH(I)) amounted to 12.4.

### 3.2. Physicochemical properties and performance of membranes modified with MgO NPs

Table 2 shows selected properties of the prepared unmodified membrane (A1) and mixed matrix membranes (A2–A6). Based on permeability values, a significant influence of the MgO NPs concentration on the water transport through membranes was observed. The permeability measured for A2 membrane, containing the lowest amount of NPs, was only slightly higher than that of the unmodified membrane (A1). In turn, the most significant increase in permeability was found in case of A6 membrane, modified with the highest concentration of MgO NPs. The permeability measured for that membrane was ca. 40% higher compared with the unmodified A1 membrane.

The data included in Table 2 revealed a correlation between permeability and contact angle values. The unmodified membrane (A1) exhibited the lowest hydrophilicity among all examined membranes. Contact angle values of modified membranes significantly decreased, as the concentration of NPs added to the membrane matrix increased and changed from  $59.2^\circ$  for the unmodified membrane to  $56.0^\circ$  for A2 membrane with the lowest concentration of MgO NPs and  $46.6^\circ$  for A6 membrane with the highest concentration of MgO NPs. The increase of hydrophilicity could be caused by the migration of MgO NPs into the top layer of a membrane as discussed by Hosseini et al. [22]. As a result of this phenomenon, MgO NPs accumulated on/near to the surface of a membrane affecting its hydrophilicity and porosity [22]. The data presented in Table 2 revealed a slight decrease of porosity in case of the mixed matrix membranes (70%–72%) in comparison with the unmodified A1 sample (75%).

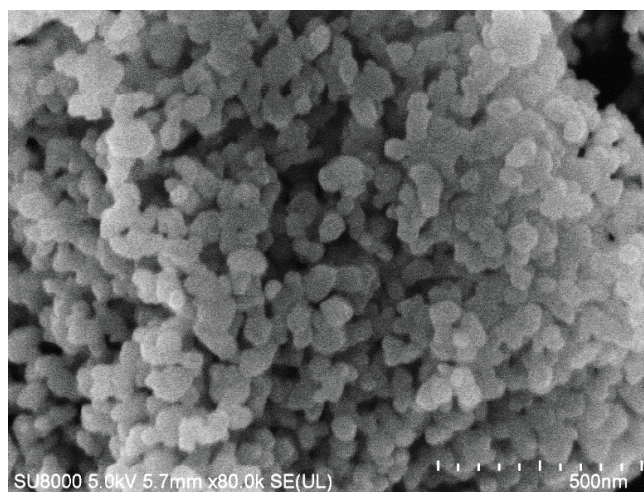


Fig. 2. SEM image of prepared MgO NPs.

Table 2  
Physicochemical properties of obtained membranes

Membrane	A1	A2	A3	A4	A5	A6
Permeability ( $\text{dm}^3/\text{m}^2 \text{ h bar}$ )	149 (10)	156 (18)	164 (19)	185 (19)	203 (2)	209 (3)
Contact angle ( $^\circ$ )	59.2 (0.6)	53.4 (0.6)	55.9 (1.7)	51.8 (0.7)	48.1 (1.3)	46.6 (1.4)
Isoelectric point	2.8 (0.11)	3.6 (0.02)	3.6 (0.08)	3.4 (0.12)	3.4 (0.12)	3.5 (0.09)
Polyethylene glycol (8 kDa) retention (%)	91 (1)	–	–	–	–	57 (9)
Porosity (%)	75 (1)	72 (1)	72 (1)	72 (1)	71 (1)	70 (1)
Roughness (nm)	1.75 (0.02)	2.84 (0.05)	2.68 (0.3)	2.30 (0.05)	2.60 (0.05)	2.62 (0.02)

The values in brackets correspond to the standard deviation (SD).

The isoelectric point (pH(I)) of A2–A6 membranes was shifted to higher pH values (3.4–3.6) compared with that of the unmodified membrane (2.8). However, no significant difference of pH(I) measured for the mixed matrix membrane with various NPs content was found.

Fig. 3 presents cross-sections of fabricated membranes recorded under SE (left column) and BSE (right column) modes. It was noted that there was no significant influence of the concentration of NPs added into the polymer matrix on the shape of pores. The unmodified A1 and the membranes

modified with MgO NPs had the same finger-like pore structures.

In order to evaluate the distribution of MgO NPs in membranes, the SEM-BSE analysis was performed (Fig. 3, right column). In case of the A2 membrane, NPs were not detected, which was explained in terms of their too low concentration. However, after increasing the dose of MgO NPs in the casting solution, some bright spots, evenly distributed throughout the cross-section of modified membranes, were observed. The uniform dispersion of NPs led to an improved

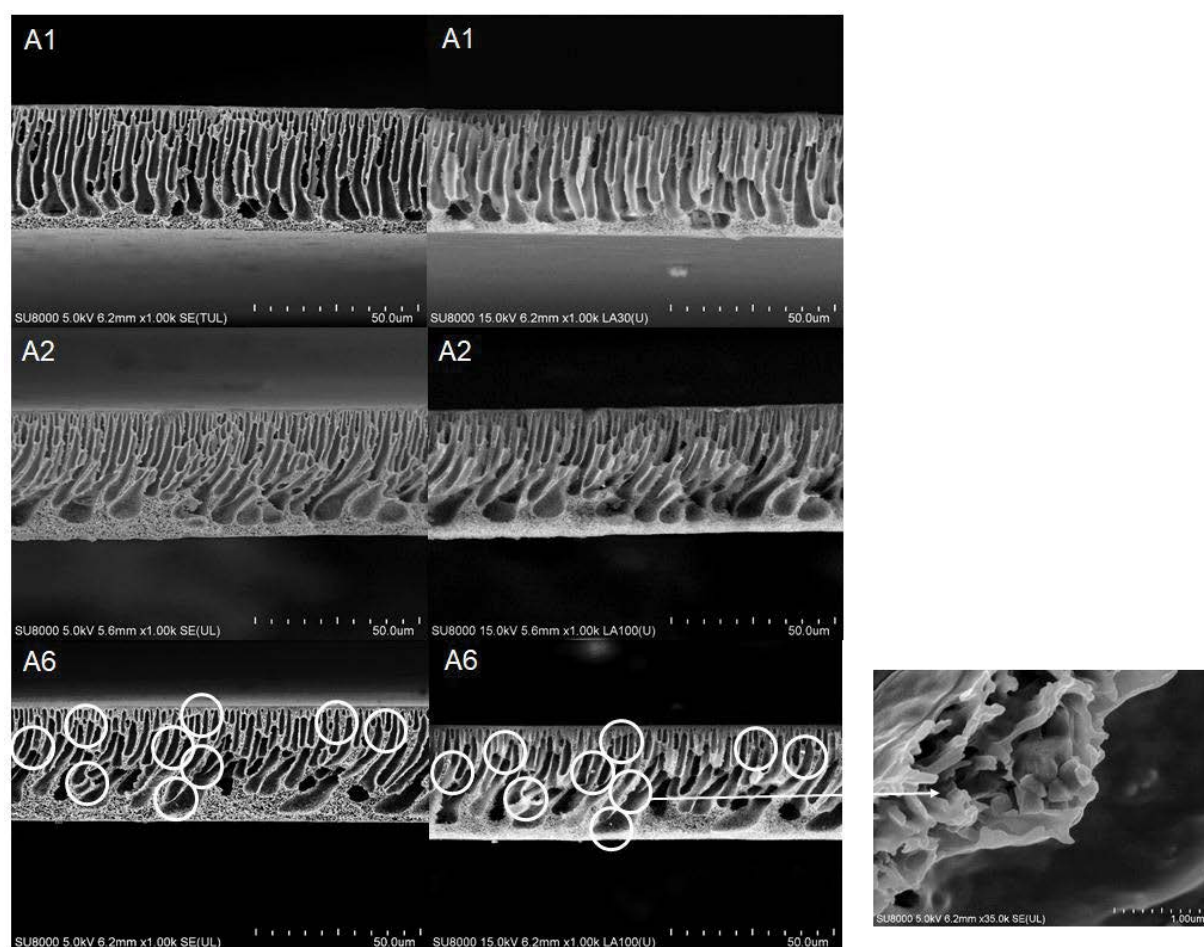


Fig. 3. SEM images of the unmodified membrane (A1), membranes modified with 0.1 wt.% MgO NPs (A2), and 5 wt.% MgO NPs (A6). Left column: SEM-SE mode, right column: SEM-BSE mode; enlargement: MgO NPs in membrane matrix (SE mode).

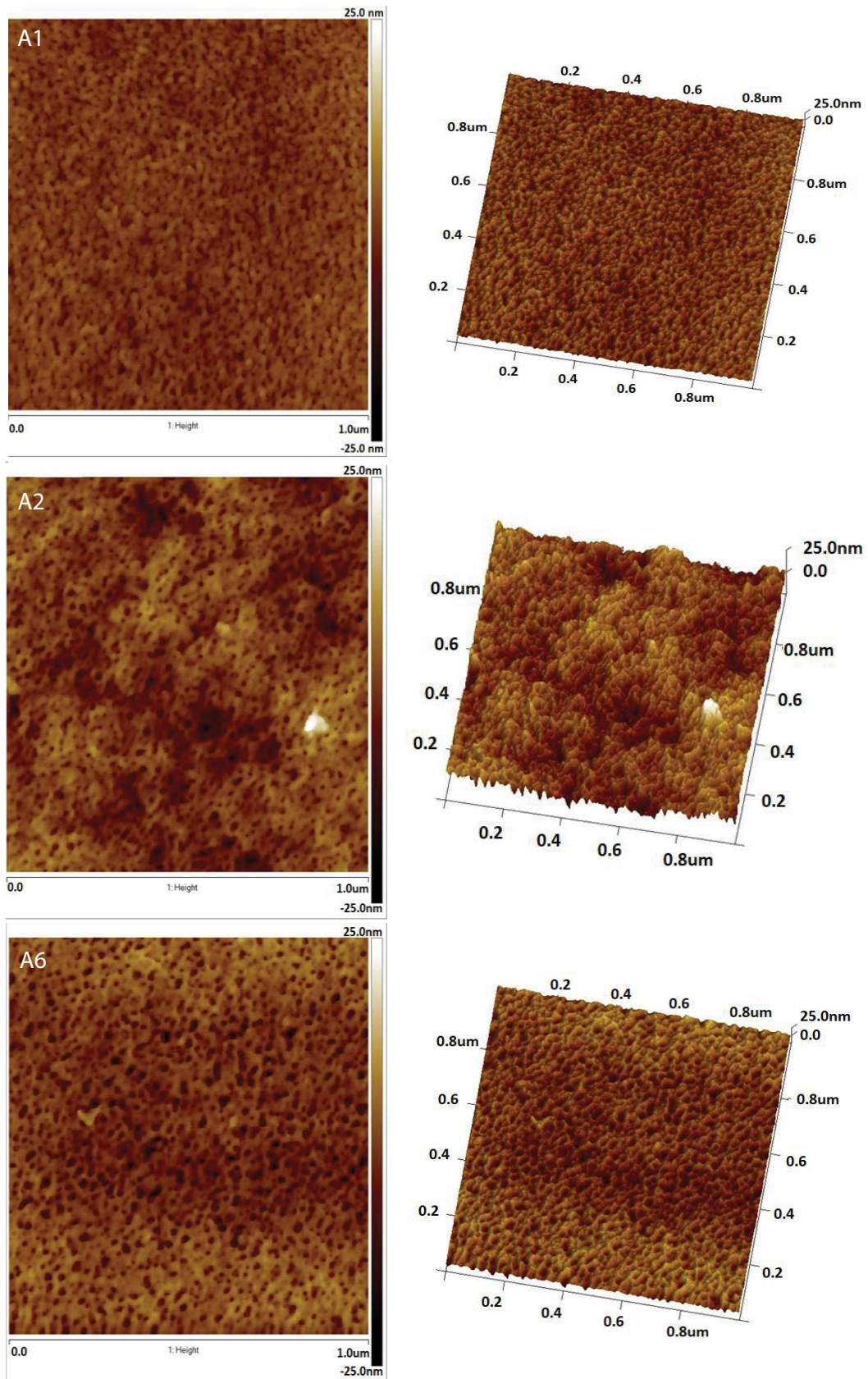


Fig. 4. AFM images of the unmodified membrane (A1) and selected membranes modified with 0.1 wt.% MgO NPs (A2), and 5 wt.% MgO NPs (A6).

permeability of water in case of the modified membranes as shown in Table 2.

The roughness of the unmodified A1 membrane and membranes containing MgO NPs was calculated based on AFM images. In case of A1, the roughness of the membrane surface was 1.75 nm (Table 2). In general, the roughness of hybrid membranes (A2–A6) was higher than that of A1. Nevertheless, no significant differences between the roughness of membranes containing various concentration of MgO NPs was observed (2.60–2.84 nm). The topography of membranes' surfaces is illustrated by AFM images (Fig. 5). The unmodified membrane had the smooth surface, with small, densely located pores. Incorporation of MgO NPs into a membrane structure had an influence on the surface undulation and appearance of mountain-like areas. Surface pores size and density observed in case of A2 and A6 were also different in comparison with the A1. In the former case the pores were packed more loosely and exhibited larger diameters than in the latter case.

Due to the visible differences in the surface structure of membranes modified with MgO NPs in relation to the unmodified membrane, the effect of the additive on the separation properties of prepared membranes was investigated. The unmodified membrane as a blank sample and the A6 membrane due to the highest permeability were selected for the investigation. Obtained results showed a decrease in the rejection of model PEG (8 kDa) from 91% for A1 to 57% for the A6 membrane. These changes may have been related to the change in the pore size and distribution observed in the AFM images (Fig. 4).

### 3.3. Antimicrobial properties of the membranes

Antimicrobial properties of the unmodified (A1) membrane and membranes containing MgO NPs were evaluated on the basis of viability of *E. coli* bacteria after 24 h of the incubation with the membranes carried out under stirring conditions (see Section 2.5). Results are summarized in Fig. 5.

An improved effect of MgO NPs on antimicrobial properties in comparison with the blank sample and A1 membrane was found. At the lowest amount of MgO NPs (A2), the growth of bacteria in relation to the blank test was inhibited by ca. 30%. The most significant influence on bacteria survival was noticed for A6 membrane containing the highest

concentration of MgO NPs. In that case the inhibition of *E. coli* growth in relation to the blank sample reached about 50%. The increase of bacterial inactivation with an increase of MgO NPs amount in a suspension was reported by Jin et al. [23]. The authors applied various concentrations of MgO NPs (1–8 mg/cm<sup>3</sup>) and *E. coli* O157:H<sub>7</sub> bacteria (10<sup>4</sup> or 10<sup>8</sup> CFU/cm<sup>3</sup>) in a trypticasein soy broth. A correlation between the concentration of MgO NPs and bacterial survival was observed. After 7 h of incubation of the 10<sup>4</sup> CFU/cm<sup>3</sup> *E. coli* suspension, the amount of bacteria decreased by ca. 5%–55% for the concentration of MgO NPs ranging from 2 to 8 mg/cm<sup>3</sup>, respectively. After 24 h of the incubation, the amount of bacteria decreased by ca. 70% for all MgO NPs doses. In case of the higher initial concentration of *E. coli* (10<sup>8</sup> CFU/cm<sup>3</sup>), the influence of MgO NPs amount on the bacteria inactivation was observed already after 24 h incubation. In this experiment, the amount of bacteria decreased by ca. 6%–82% for MgO NPs concentrations of 2–8 mg/cm<sup>3</sup>, respectively. The mechanism of antibacterial action of MgO NPs can be attributed to the production of reactive oxygen species (ROS) [24,25]. Leung et al. [26] also postulated a non-ROS mediated toxicity mechanism for MgO NPs, although this pathway was claimed to be of a minor importance [26]. The ROS-based mechanism is associated with peroxidation of l- $\alpha$ -phosphatidylethanolamine and lipopolysaccharide located in outer membrane and in cell walls of *E. coli* bacteria, respectively. The non-ROS mechanism is based on the removal of phosphate (PO<sub>3</sub><sup>4-</sup>) from bacteria cells. The mechanism based on the attachment of MgO NPs to the bacteria surface through various types of interactions, including Van der Waals, electrostatic, hydrophobic, and receptor–ligand interactions affecting the cell membrane elasticity was also proposed. Nonetheless, the authors concluded that the pathways of MgO antibacterial action toward *E. coli* depended on the type of MgO NPs, pH changes, and release of Mg<sup>2+</sup> ions [26].

## 4. Conclusions

In this study the positive influence of MgO NPs on transport properties and antimicrobial activity of polyethersulfone membranes obtained by the wet phase inversion method was revealed. It was found that an increase of the amount of nanomaterial in the casting solution resulted in an improvement of permeability of the obtained membranes. The highest value of this parameter was reached for A6 membrane (209 dm<sup>3</sup>/m<sup>2</sup> h bar). The improvement of permeability was associated with a decrease of contact angle values corresponding to the enhancement of hydrophilicity, as well as an increase of the size of pores visible on the AFM images of the membrane surface. Nonetheless, the overall porosity of membranes decreased with the increasing MgO NPs load. The analysis of antimicrobial properties of membranes showed a significant influence of MgO NPs addition on *E. coli* bacteria survival. The highest degree of inhibition of bacterial growth in the model suspension was noted for A6 membrane containing the highest concentration of the nanomodifier (5 wt.%).

### Symbols

- $\lambda$  — Wavelength of CuK $\alpha$  radiation ( $\lambda = 1.54056 \text{ \AA}$ )  
 $K$  — Shape factor ( $K = 0.9$ )

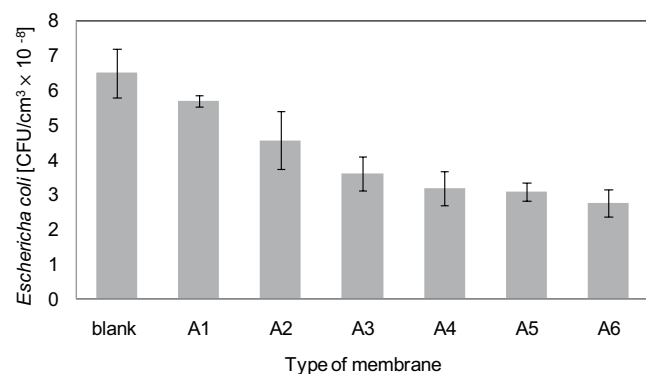


Fig. 5. *Escherichia coli* survival after 24 h of incubation in the presence of the modified PES membranes containing various amount of MgO NPs.

$m_{\text{dry}}$	—	Weight of dry membrane samples, g
$m_{\text{wet}}$	—	Weight of wet membrane samples, g
$X$	—	Number of colonies visible on the Petri dish
$Y$	—	Total dilution factor
$Z$	—	Volume of bacteria suspension placed on the agar (0.3 cm <sup>3</sup> )
$\beta$	—	Full width at the half maximum height of the diffraction peak
$\rho_p$	—	Polymer (PES) density, g/cm <sup>3</sup>
$\rho_w$	—	Water density, g/cm <sup>3</sup>

## References

- [1] M.T. Ravanchi, T. Kaghazchi, A. Kargari, Application of membrane separation processes in petrochemical industry: a review, *Desalination*, 235 (2009) 199–244.
- [2] J. Nuortila-Jokinen, A. Kuparinen, M. Nyström, Tailoring an economical membrane process for internal purification in the paper industry, *Desalination*, 119 (1998) 11–19.
- [3] G. Ciardelli, L. Corsi, M. Marcucci, Membrane separation for wastewater reuse in the textile industry, *Resour., Conserv. Recycl.*, 31 (2000) 189–197.
- [4] A.K. Pabby, S.S.H. Rizvi, A.M. Sastre, *Handbook of membrane separations: chemical, pharmaceutical, food, and biotechnological applications*, Taylor & Francis Group, Boca Raton, FL, 2015.
- [5] D. Kim, S. Jung, J. Sohn, H. Kim, S. Lee, Biocide application for controlling biofouling of SWRO membranes — an overview, *Desalination*, 238 (2009) 43–52.
- [6] G. Petrucci, M. Rosellini, Chlorine dioxide in seawater for fouling control and post-disinfection in potable water works, *Desalination*, 182 (2005) 283–291.
- [7] B. Meyer, Approaches to prevention, removal and killing of biofilms, *Int. Biodeterior. Biodegrad.*, 51 (2003) 249–253.
- [8] K.C. Khulbe, C. Feng, T. Matsuura, The art of surface modification of synthetic polymeric membranes, *J. Appl. Polym. Sci.*, 115 (2010) 855–895.
- [9] V. Kochkodan, D.J. Johnson, N. Hilal, Polymeric membranes: surface modification for minimizing (bio)colloidal fouling, *Adv. Colloid Interface Sci.*, 206 (2014) 116–140.
- [10] J. Kim, B. Van der Bruggen, The use of nanoparticles in polymeric and ceramic membrane structures: review of manufacturing procedures and performance improvement for water treatment, *Environ. Pollut.*, 158 (2010) 2335–2349.
- [11] J.H. Choi, J. Jegal, W.N. Kim, Fabrication and characterization of multi-walled carbon nanotubes/polymer blend membranes, *J. Membr. Sci.*, 284 (2006) 406–415.
- [12] L.Y. Ng, A.W. Mohammad, C.P. Leo, N. Hilal, Polymeric membranes incorporated with metal/metal oxide nanoparticles: a comprehensive review, *Desalination*, 308 (2013) 15–33.
- [13] H.L. Richards, P.G.L. Baker, E. Iwuoha, Metal nanoparticle modified polysulfone membranes for use in wastewater treatment: a critical review, *J. Surf. Eng. Mater. Adv. Technol.*, 2 (2012) 183–193.
- [14] I. Sawada, R. Fachrul, T. Ito, Y. Ohmukai, T. Maruyama, H. Matsuyama, Development of a hydrophilic polymer membrane containing silver nanoparticles with both organic antifouling and antibacterial properties, *J. Membr. Sci.*, 387–388 (2012) 1–6.
- [15] I. Marinov, Y. Ivanov, K. Gabrovska, T. Godjevargova, Amperometric acetylthiocholine sensor based on acetylcholinesterase immobilized on nanostructured polymer membrane containing gold nanoparticles, *J. Mol. Catal. B: Enzym.*, 62 (2010) 66–74.
- [16] S.Y. Lee, H.J. Kim, R. Patel, S.J. Im, J.H. Kim, B.R. Min, Silver nanoparticles immobilized on thin film composite polyamide membrane: characterization, nanofiltration, antifouling properties, *Polym. Adv. Technol.*, 18 (2007) 562–568.
- [17] M. Ben-Sasson, K.R. Zodrow, Q. Genggeng, Y. Kang, E.P. Giannelis, M. Elimelech, Surface functionalization of thin-film composite membranes with copper nanoparticles for antimicrobial surface properties, *Environ. Sci. Technol.*, 48 (2014) 384–393.
- [18] Y. Cai, C. Li, D. Wu, W. Wang, F. Tan, X. Wang, P.K. Wong, X. Qiao, Highly active MgO nanoparticles for simultaneous bacterial inactivation and heavy metal removal from aqueous solution, *Chem. Eng. J.*, 312 (2017) 158–166.
- [19] G. Moussavi, M. Mahmoudi, Removal of azo and anthraquinone reactive dyes from industrial wastewaters using MgO nanoparticles, *J. Hazard. Mater.*, 168 (2009) 806–812.
- [20] Z.X. Tang, B.F. Lv, MgO nanoparticles as antibacterial agent: preparation and activity, *Braz. J. Chem. Eng.*, 31 (2014) 591–601.
- [21] T. Arumugham, N.J. Kaleekkal, D. Rana, M. Doraiswamy, Separation of oil/water emulsions using nano MgO anchored hybrid ultrafiltration membranes for environmental abatement, *J. Appl. Polym. Sci.*, 133 (2016), 42848, 12 pages.
- [22] S.M. Hosseini, E. Bagheripour, M. Ansari, Adapting the performance and physico-chemical properties of PES nanofiltration membrane by using of magnesium oxide nanoparticles, *Korean J. Chem. Eng.*, 34 (2017) 1774–1780.
- [23] T. Jin, Y. He, Antibacterial activities of magnesium oxide (MgO) nanoparticles against foodborne pathogens, *J. Nanopart. Res.*, 12 (2011) 6877–6885.
- [24] J. Sawai, T. Yoshikawa, Quantitative evaluation of antifungal activity of metallic oxide powders (MgO, CaO and ZnO) by an indirect conductimetric assay, *J. Appl. Microbiol.*, 96 (2004) 803–809.
- [25] K. Krishnamoorthy, G. Manivannan, S.J. Kim, K. Jeyasubramanian, M. Premanathan, Antibacterial activity of MgO nanoparticles based on lipid peroxidation by oxygen vacancy, *J. Nanopart. Res.*, 14 (2012) 1063.
- [26] Y.H. Leung, A.M. Ng, X. Xu, Z. Shen, L.A. Gethings, M.T. Wong, C.M. Chan, M.Y. Guo, Y.H. Ng, A.B. Djurišić, P.K. Lee, W.K. Chan, L.H. Yu, D.L. Phillips, A.P. Ma, F.C. Leung, Mechanisms of antibacterial activity of MgO: non-ROS mediated toxicity of nanoparticles towards *Escherichia coli*, *Small*, 10 (2014) 1171–1183.